Journal of Drug Delivery Science and Technology 104 (2025) 106518

Contents lists available at ScienceDirect

Journal of Drug Delivery Science and Technology

journal homepage: www.elsevier.com/locate/jddst

Smart hyaluronated micelles to enhance a gemcitabine prodrug efficacy

Ilaria Andreana [a], Valeria Bincoletto [a], Caterina Ricci [b], Iris Chiara Salaroglio [c], Maela Manzoli [a], Beatrice Zurletti [a], Jessica Milone [a], Barbara Rolando [a], Elena Del Favero [b], Chiara Riganti [c], Pietro Matricardi [d], Barbara Stella [a], Silvia Arpicco [a,*]

[a] Department of Drug Science and Technology, University of Turin, Via Pietro Giuria 9, 10125, Turin, Italy
[b] Department of Medical Biotechnology and Translational Medicine, University of Milan, Via Fratelli Cervi 93, 20054, Milan, Italy
[c] Department of Oncology, Interdepartmental Center of Molecular Biotechnology "Guido Tarone", University of Turin, Via Nizza 44, 10126, Turin, Italy
[d] Departments of Drug Chemistry and Technologies, Sapienza University of Rome, Piazzale Aldo Moro 5, 00185, Rome, Italy

ARTICLE INFO

Keywords:
Hyaluronic acid
4-(N)-Stearoyl gemcitabine
Micelles
CD44 receptor
Targeted drug delivery

ABSTRACT

Self-assembling drug delivery systems have drawn attention over recent decades thanks to their versatility and easy preparation processes. Of the various nanocarriers available, micelles are able to self-assemble from an amphiphilic molecule in an aqueous solution, making them simple to prepare. In this work, 1,2-distearoyl-*sn*-glycero-3-phosphoethanolamine-N-[methoxy(polyethylene glycol)-2000] (PEG-DSPE) was utilized to prepare lipid-based micelles for the encapsulation of a gemcitabine prodrug, GemC18, with the aim of improving its anticancer activity. Furthermore, an active targeting strategy was achieved by preparing Gem-C18-loaded PEG-DSPE micelles in the presence of a hyaluronic acid (4800 or 14,800 Da) (HA)-phospholipid conjugate (HA-DPPE) to provide actively targeted mixed micelles. This study presents the characterization of the mixed micelles, from basic characteristics (size, PDI, and zeta potential) to complex molecular structure (FESEM, X-ray diffraction, SAXS), and demonstrates that the presence of the HA-conjugate does not alter the physicochemical properties of the PEG-DSPE micelles. The mixed micelles display a size of below 100 nm, a negative zeta potential of −30 mV, and a high encapsulation efficiency (above 90 %). Finally, their preferential uptake, and consequently their cytotoxicity on cancer cell lines that overexpress the HA-specific receptor (CD44), has been assessed and confirmed using competition assays.

1. Introduction

Many chemotherapeutic agents exhibit various types of systemic toxicity and side effects that are caused by their poor accumulation in tumor tissues. Nanotechnologies have therefore been developed to increase tumor accumulation and reduce the systemic adverse effects of drug distribution in normal tissues [1–3]. Drug delivery systems of various nature (*e.g.* liposomes, polymer, and inorganic nanoparticles) have undergone extensive studies in order to improve their ability to encapsulate and deliver active molecules, including small molecules, genetic material, and imaging agents [4,5]. Micelles are one of the huge number of well-characterized nanocarriers, and are beginning to be considered one of the most attractive strategies [6]. Micelles are colloidal particles, ranging from 5 to 100 nm, formed *via* the self-assembly of amphiphilic molecules in aqueous solution, distinguishing them as a simple drug delivery system. The phenomenon of micelle formation starts when the concentration of the amphiphilic molecule exceeds a precise threshold of concentration, defined as the critical micelle concentration [7,8]. Micelles usually display smaller sizes than other drug delivery systems, and have been extensively investigated for the delivery of poorly soluble molecules [9–11], which can be incorporated into the hydrophobic cores of these structures after dispersion in an aqueous medium [12]. Amphiphilic copolymers can spontaneously form core-shell micelles made of a hydrophilic shell and a hydrophobic core, into which a hydrophobic drug can be easily incorporated [13,14]. Moreover, interest in lipid-based micelles has increased

* Corresponding author. Via Pietro Giuria 9, 10125, Torino, Italy.
E-mail addresses: ilaria.andreana@unito.it (I. Andreana), valeria.bincoletto@unito.it (V. Bincoletto), caterina.ricci@unimi.it (C. Ricci), irischiara.salaroglio@unito.it (I.C. Salaroglio), maela.manzoli@unito.it (M. Manzoli), beatrice.zurletti@unito.it (B. Zurletti), jessica.milone@edu.unito.it (J. Milone), barbara.rolando@unito.it (B. Rolando), elena.delfavero@unimi.it (E. Del Favero), chiara.riganti@unito.it (C. Riganti), pietro.matricardi@uniroma1.it (P. Matricardi), barbara.stella@unito.it (B. Stella), silvia.arpicco@unito.it (S. Arpicco).

https://doi.org/10.1016/j.jddst.2024.106518
Received 28 August 2024; Received in revised form 21 November 2024; Accepted 10 December 2024
Available online 10 December 2024

in recent years thanks to their biodegradability and biocompatibility. For example, a potent water-insoluble tyrosine kinase inhibitor showed enhanced water solubility and cellular uptake, compared to the free molecule, *via* incorporation into poly(ethylene glycol) (PEG)-lipid-based micelles [15]. The ability of PEG–phosphatidylethanolamine (PE) conjugates to form micelles in an aqueous environment was observed as early as 1994. The use of a lipid moiety as the hydrophobic block improves micelles stability thanks to the strong hydrophobic interactions between the alkyl chains of the phospholipids [16]. Moreover, the presence of PEG on micelle surfaces increases their circulation time *in vivo* by preventing their recognition by opsonins, and thus reducing their clearance. While PEG is the most commonly used hydrophilic block, because of its "stealth" ability, the composition of the hydrophobic block can be tailored to improve the encapsulation of lipophilic drugs. In recent times, the amphiphilic polymer 1,2-distearoyl-*sn*-glycero-3-phosphoethanolamine-N-[methoxy(polyethylene glycol)-2000] (PEG-DSPE) has often been used in nanomedicine to prepare nanocarriers because of its ability to form micellar structures in water. For example, PEG-DSPE, with a terminal amino group, has been covalently combined with a fullerene structure and self-assembled into micelles to deliver doxorubicin, thus enhancing the drug's *in vivo* efficacy and safety [17]. As is well known, the presence of the PEG shell prolongs the circulation time of drug delivery systems *in vivo* [18,19]. In addition, micelles can accumulate at tumor sites as their nanoscale structures can exploit the enhanced permeability and retention (EPR) effect [20–22].

However, the aspecific accumulation of drug delivery systems has underlined the urgent need for targeting strategies. Indeed, specific molecules on the nanocarrier surface can promote accumulation into organs or tissues and consequently improve the therapeutic effects [23].

Polysaccharides are considered to be amongst the most important materials when designing novel actively targeted nanosystems. Hyaluronic acid (HA) is a natural polysaccharide composed of alternating units of D-glucuronic acid and N-acetyl-D-glucosamine, linked *via* β-1,3- and β-1,4-glycosidic bonds. HA is a promising component, from a pharmaceutical standpoint, because it is biocompatible, biodegradable, nontoxic and non-immunogenic. It has also been used as a targeting moiety as it can bind the CD44 receptor, which is overexpressed on many tumor cells [24]. Moreover, HA contains several chemical groups to which other components can be conjugated. Thanks to all these features, HA has been widely employed in the development of drug delivery systems, in recent years, having been used, as such or as a ligand, in different types of nanosystems, to prepare nanoplatforms for actively targeted drugs, genes and diagnostic agents [25].

The anticancer drug gemcitabine, a cytidine analogue, is the first-line treatment for pancreatic adenocarcinoma. However, its clinical outcomes suffer from rapid metabolism that leads to drug administration in very high doses and the onset of acquired drug resistance [26]. A great deal of effort has therefore been made to overcome these limitations, with the identification of new derivatives with improved effects; one of these derivatives, the lipophilic prodrug 4-(N)-stearoyl gemcitabine (GemC18), has shown improved pharmacokinetics and superior antitumor efficacy [27]. Thanks to its suitable features, GemC18 has been incorporated in nanosystems of diverse nature to improve its activity, with these systems including liposomes [27], microparticles [28], and nano-onions [29]. GemC18 has also been exploited for incorporation into different types of micelles, like acid-sensitive [30], polymeric [31], and lipid-based micelles [32].

In this work, a very low amount of HA-phospholipid conjugate (HA-DPPE), at two different HA molecular weights (4800 or 14,800 Da) was added, during the preparation of PEG-DSPE micelles loaded with GemC18 to set up an active targeting strategy. The mixed micelles self-assembled, exposing HA on their surfaces, making it available for interaction with the CD44 receptor. The micelles were characterized, from basic characteristics to more complex methods including cellular uptake and cytotoxic activity towards pancreatic cancer cells with low (Capan-1) and high (Panc-1) CD44-receptor expression.

2. Materials and methods

2.1. Materials and general procedures

Sodium hyaluronate (HA) (4800 and 14,800 Da) was purchased from Lifecore Biomedical (Chaska, Minnesota, USA). 1,2-distearoyl-*sn*-glycero-3-phosphoethanolamine-N-[methoxy(polyethylene glycol)-2000] (ammonium salt) (PEG-DSPE), 1,2-dipalmitoyl-*sn*-glycero-3-phosphoethanolamine (DPPE), Nile Red, 0.22 μm nylon filters, pyrene and solvents (analytical grade) were obtained from Merck (Milan, Italy). Solvent evaporation was carried out on a rotating evaporator (Heidolph Laborota 400, Heidolph Instruments, Schwabach, Germany) equipped with a vacuum pump (Diaphragm Vacuum Pump DC-4). Spectra-Por® 12–14,000 molecular weight cut off dialysis membrane were obtained from Thermo Fisher Scientific (Monza, Italy).

Conjugates between DPPE and HA (HA_{4800}-DPPE and HA_{14800}-DPPE) were prepared using the method described in Arpicco et al. [33], with minor modifications. Briefly, HA (4800 or 14,8000 Da) was dissolved in a methanol/dimethyl sulfoxide mixture (1:1 v/v). An equimolar amount of DPPE was dissolved in a methanol/chloroform mixture (1:1 v/v) and added to the HA solution under stirring at 60 °C. The pH was adjusted to 4.5 using acetic acid and the suspension was stirred for 2 h at 60 °C. Sodium triacetoxyborohydride, dissolved in the methanol/chloroform mixture, was then added dropwise. The reaction was allowed to proceed for 96 h at 60 °C under continuous stirring. The organic solvents were removed under reduced pressure and then the mixture was dialyzed against water. The final product was purified by chromatography and lyophilized; ^{1}H NMR analysis confirmed the formation of the conjugate. The gemcitabine lipophilic prodrug (GemC18) was synthesized according to Immordino et al. [27].

2.2. Critical micelle concentration measurement

Critical micelle concentration (CMC) was measured by fluorescence spectroscopy using pyrene as a fluorescent dye [34]. Briefly, a stock solution of 2.00×10^{-5} M of pyrene was prepared in acetone; 50 μL aliquots of the solution were added to a series of glass tubes and acetone was completely evaporated by rotary evaporation under reduced pressure. Different amounts of PEG-DSPE, HA_{4800}-DPPE, HA_{14800}-DPPE, PEG-DSPE/HA_{4800}-DPPE or PEG-DSPE/HA_{14800}-DPPE ranging from 1.00×10^{-8} to 1.27×10^{-3} M were separately added to each tube to obtain a final pyrene concentration of 2.00×10^{-6} M. Each sample was incubated at 60 °C for 20 min and equilibrated overnight at room temperature. After filtration through a 0.22 μm nylon syringe filter, the fluorescent spectra of each sample were analyzed using a spectrofluorometer EnSight HH3400 (PerkinElmer, Inc., Waltham, Massachusetts, USA) equipped with a data recorder Kaleido 1.2 at the excitation wavelength of 339 nm, and the emission spectra were monitored from 360 to 450 nm. Excitation slit widths were set at 373, 384 and 390 nm. Results are expressed as the correlation between the log[phospholipid] and intensity ratio of either I_{373}/I_{384} or I_{390}.

2.3. Micelle preparation

PEG micelles (PEG-M) were prepared *via* the hydration and sonication of a PEG-DSPE film. Briefly, 2 mg of PEG-DSPE were dissolved in chloroform and evaporated using a rotary evaporator; the resulting thin film was dried under vacuum overnight. The film was hydrated with 3 mL of MilliQ® water at 60 °C and incubated for 10 min. The suspension was then cooled and sonicated in an ice bath with a probe sonicator VCX400 (Sonics & Materials Inc., Milan, Italy) for 10 min with pulses of 3 s on and 3 s off.

Mixed micelles (PEG-M/HA_{4800} or PEG-M/HA_{14800}) were prepared by adding a 1 % molar ratio of HA_{4800}-DPPE or HA_{14800}-DPPE to the

aqueous solution during the hydration of the PEG-DSPE film.

GemC18-loaded micelles were prepared by adding 500 μL of GemC18 solution (1 mg/mL in methanol) to the chloroform solution of PEG-DSPE (2 mg/200 μL); the solvents were evaporated under reduced pressure to obtain a homogeneous thin drug-lipid film. To prepare GemC18-PEG-M/HA-DPPE$_{4800}$ or GemC18-PEG-M/HA-DPPE$_{14800}$, the conjugates were dissolved in MilliQ® water (1 mg/mL) and the film was hydrated with 3 mL of MilliQ® water containing 60 μL of HA$_{4800}$-DPPE or 110 μL of HA$_{14800}$-DPPE aqueous solution. The resulting micelle suspension was purified *via* filtration through a 0.22 μm nylon syringe filter.

Fluorescently labelled micelles were prepared as well by adding 40 μL of a Nile Red solution (200 μg/mL) in dichloromethane/acetone during thin lipid film preparation.

Drug-loaded HA-DPPE micelles were prepared in a similar manner using a solution of HA$_{4800}$-DPPE or HA$_{14800}$-DPPE (0.7 mg/mL) in MilliQ® water to hydrate the GemC18 film.

2.4. Physicochemical characterization of micelles

The mean particle hydrodynamic diameter and polydispersity index (PDI) of the different micelle samples were determined at 25 °C *via* quasi-elastic light scattering (QELS) using a nanosizer (Zetasizer Pro, Malvern Inst., Malvern, UK). The selected angle was 173° and the measurements were performed on undiluted sample at pH 6.5. Each measurement was performed in triplicate. The particle surface charge of the preparations was investigated *via* zeta potential measurement at 25 °C using the Smoluchowski equation and the Zetasizer Pro directly on the pure samples. Each value is the average of three measurements.

The encapsulation efficiency (EE) and drug loading (DL) of GemC18-loaded micelles were determined by HPLC; samples were diluted 1:10 with acetonitrile to extract the incorporated drug. HPLC analysis was performed on a HP 1200 chromatograph system (Agilent Technologies, Palo Alto, California, USA) equipped with an injector (Rheodyne, Cotati, California, USA), a quaternary pump (model G1311A), a membrane degasser (model G1322A), a multiple wavelength UV detector (MWD, model G1365D) and a fluorescence detector (FL, model G1321A) integrated into the HP1200 system. Data were processed using a HP ChemStation system (Agilent Technologies). The analytical column was a AQUASIL C18 (200 × 4.6 mm, 5 μm; Thermo); the mobile phase consisted of acetonitrile/water/TFA, 90/9.9/0.1 (v/v/v), at a flow-rate of 1 mL/min. The injection volume was 20 μL (Rheodyne, Cotati, California, USA). The column effluent was monitored at 250 nm and 292 nm referenced against 800 nm wavelength.

GemC18 EE and DL were calculated as follows:

$$EE(\%) = \frac{A}{B} \times 100$$

where A is the amount of incorporated drug after micelle purification and B is the initial added amount of GemC18.

$$DL(\%) = \frac{C}{D} \times 100$$

where C is the weight of incorporated drug after micelle purification and D is the total micelle weight.

2.5. In vitro release study

To evaluate *in vitro* GemC18 release, 3 mL of each sample (GemC18-PEG-M, GemC18-PEG-M/HA$_{4800}$ and GemC18-PEG-M/HA$_{14800}$) were placed into a dialysis bag immersed in 300 mL of PBS 1 mM (pH 7.4) at 37 °C, and aliquots (100 μL) were withdrawn at predetermined time intervals (0, 0.5, 1, 3, 5, 24, 48 and 72 h). The amount of GemC18 content was determined by HPLC, as previously described.

2.6. Small angle X-ray scattering

SAXS experiments were performed at the European Synchrotron Radiation Facility (ESRF), at ID02 beamline (DOI:10.15151/ESRF-ES-1351189712). 30 μL of each sample were loaded into capillaries (KI-beam, ENKI, Concesio, Italy) and measured at 25 ± 1°C. The 2D spectra reported the scattered radiation as a function of the angle θ. To avoid any radiation damage, 10 frames with a short exposure time (0.1 s) were acquired, compared, and averaged. After normalization, background subtraction, and angular regrouping the 1D SAXS intensity profiles were obtained and reported as a function of the momentum transfer $q=(4\pi/\lambda)\sin(\theta/2)$ where $\lambda = 1$ Å is the radiation wavelength. To investigate a wide q region, $0.008\ \text{Å}^{-1} \leq q \leq 0.5\ \text{Å}^{-1}$, SAXS spectra relative to different q ranges, modifying the sample-detector distance (1 m and 10 m), were acquired, compared and connected. SAXS data were analyzed with GENFIT software [35] to derive micellar structural parameters, size, shape and internal arrangement.

2.7. Power X-ray diffraction

Powder X-Ray Diffraction (PXRD) patterns were collected by using a PW3050/60 X'Pert PRO MPD diffractometer (PANalytical) working in Bragg–Brentano geometry, equipped with a high-powered ceramic tube PW3373/10 LFF with a Cu anode as a source (Cu Kα radiation λ = 1.5406) with a Ni filter to attenuate Kβ. Scattered photons were collected by a real time multiple strip (RTMS) X'celerator detector. Data were acquired in the $3° \leq 2\theta \leq 60°$ angular range, with 0.02° 2θ steps. The as received samples in the form of powders were examined using a spinning sample holder to minimize preferred orientations.

For the analyses, two drops of each sample were deposited onto aluminum stubs coated with a conducting adhesive and then left to dry in the air at room temperature. The dried samples underwent Cr metallization (ca. 5 nm) by employing an Emitech K575X sputter coater (Quorumtech, Laughton, 226 East Sussex, UK) to avoid charging effects and inserted into the instrument chamber using a motorized procedure.

2.8. Field Emission Scanning Electron Microscopy

Field Emission Scanning Electron Microscopy (FESEM) analyses were performed by a Tescan S9000G FESEM 3010 microscope (Tescan Orsay Holding a.s., Brno- Kohoutovice, Czech Republic) working at 30 kV, equipped with a high brightness Schottky emitter and fitted with Energy Dispersive X-ray Spectroscopy (EDS) analysis by an Ultim Max Silicon Drift Detector (SDD, Oxford, UK). For the analysis, two drops of the prepared sample were deposited onto an aluminum stub coated with a conducting adhesive and subsequently left to dry in the air at room temperature. The dried sample was submitted to Cr metallization (ca. 5 nm) using an Emitech K575X sputter coater (Quorumtech, Laughton, East Sussex, UK) to avoid charging effects and then inserted into the chamber by a motorized procedure. Histogram of the particle size distribution built for the PEG-M/HA$_{14800}$ sample was obtained by considering a representative number of particles and the mean particle diameter (d_m) was calculated by applying the following equation:

$d_m = \Sigma d_i n_i / \Sigma n_i$, being n_i the number of particles with diameter d_i.

2.9. Cell lines culture and characterization

Human pancreatic adenocarcinoma cells Capan-1 and PANC-1 were purchased from ATCC (Manassas, Virginia, USA) and maintained in their respective medium (DMEM for Capan-1, RPMI-16140 for PANC-1, by Invitrogen Life Technology, Milan, Italy), containing 1 % v/v penicillin-streptomycin and 10 % fetal bovine serum (Merck). The surface amount of CD44, the receptor for HA, was evaluated by flow

cytometry as previously described [36], using a Guava Millipore flow cytometer equipped with EasyCite software (Millipore, Bedford, Massachusetts, USA). Capan-1 and PANC-1 cells were classified as CD44-low and high expressing cells [29].

2.10. Micelle uptake

1×10^5 cells were seeded into a 96-well black plate in 200 μL medium, and incubated for 1, 3, 6, and 24 h with Nile Red-loaded micelles without HA (NR-PEG-M) or with HA (NR-PEG-M/HA_{4800} or NR-PEG-M/HA_{14800}), at final dilutions of 1:2, 1:5 and 1:10. When indicated, a saturating amount of blocking anti-CD44 antibody (#ab157107; Abcam, Cambridge, UK; diluted 1/100) or HA (100 μM) was added to the cells incubated with micelles diluted 1:2. After two washing with PBS, cells were detached with trypsin/EDTA, collected in 300 μL PBS and sonicated. A 50 μL aliquot was used to measure the cellular proteins (BCA kit); the remaining samples were transferred into a dark-wall 96 well plate and the intracellular fluorescence, corresponding to the amount of uptake of Nile Red, was read at λ excitation 559 nm and λ emission 635 nm, using a Synergy HT Microplate Reader. The results were expressed as fluorescence units (FU)/mg cellular proteins. In each experimental set, the autofluorescence – *i.e.* the fluorescence of untreated cells – was 0.26 ± 0.6 nmol/mg for Capan-1 cells and 0.28 ± 0.6 nmol/mg for PANC-1 cells and was subtracted from the fluorescence of any other experimental conditions.

2.11. Cell viability

1×10^4 cells were seeded into a 96-well white plate and incubated for 24, 48 and 72 h with the fresh medium, medium containing free gemcitabine (Gem), free GemC18 or GemC18-loaded micelles (with or without HA), containing a concentration of GemC18 corresponding to 100 nM, 1 μM, 10 μM. When indicated, the cells treated with 10 μM GemC18-loaded micelles containing HA_{4800}-DPPE or HA_{14800}-DPPE were co-incubated for 72 h with blocking anti-CD44 antibody diluted 1/100 or HA (100 μM). Cell viability was measured by a chemiluminescent-based commercial kit (ATPlite Luminescence Assay System, PerkinElmer, Waltham, MA), using a Synergy HT Microplate Reader, setting the luminescence units detected in untreated cells as 100 %. The luminescence units of each condition were expressed as percentage versus untreated cells.

2.12. Statistical analysis

Data in the text and figures are provided as means ± SD. The results were analyzed by a one-way analysis of variance (ANOVA) and Tukey's test. $p < 0.05$ was considered significant.

3. Results and discussion

3.1. Preparation and characterization of micelles

HA is widely used as a platform for the specific delivery of anticancer drugs because of its ability to recognize the specific CD44 receptor, which is overexpressed on the surface of several tumors [37]. Moreover, HA is biocompatible, biodegradable, nontoxic and non-immunogenic. We previously synthesized HA-phospholipid conjugates that were used for the preparation of decorated liposomes actively targeted towards CD44-overexpressing cancer cells [33,38]. Furthermore, we demonstrated the potential cryoprotective effect that the HA-DPPE conjugate has on liposomes and poly(lactic-*co*-glycolic acid) (PLGA) nanoparticles; the addition of the conjugate during the formulation of lipid or polymer-based nanosystems led to the physicochemical properties of the redispersed sample being retained after lyophilization [39].

In this work, we initially proposed the use of HA-DPPE conjugates prepared using HA at two different molecular weights (4800 and 14,800 Da) for the preparation of micelles.

We decided to investigate the ability of the micelles as a vehicle for the specific delivery of GemC18 towards pancreatic cancer cells, overexpressing the specific HA CD44 receptor. In previous works, we demonstrated that GemC18, a lipophilic prodrug of Gem that is currently the gold standard treatment for pancreatic cancer, displays significant anticancer activity [27,29].

Here, GemC18-loaded HA-DPPE formulations showed an encapsulation efficiency of around 60 % and fast drug release; 60 % of GemC18 was released after 1 h in PBS at 37 °C. To improve GemC18 loading and stability, we decided to use PEG-DSPE as the main component for micelle preparation because of its well-known ability to form micelles in aqueous media [16]. A similar approach has previously been exploited to form self-assembled mixed micelles that incorporated GemC18 and promoted slow drug release and preferential drug accumulation in the tumor *via* the EPR effect [32]. Moreover, to improve the targeting ability of the GemC18-loaded micelles towards pancreatic cancer cells overexpressing the CD44 receptor, we initially decided to test HA-DPPE at different amounts ranging from 1 % to 20 % of PEG-DSPE. The 1 % molar ratio of HA-DPPE (4800 or 14,800 Da) was then chosen to obtain mixed micelles (Fig. 1) with suitable physico-chemical characteristics.

To the best of our knowledge, for the first time the use of a very low amount of HA-lipid conjugate has been proposed for the preparation of actively targeted micelles.

CMC is a key parameter as, it not only indicates the solubilization efficiency of micelles, but also demonstrates their stability. To determine the CMC of micelles, the pyrene method was chosen for its versatility and easy applicability. The CMC of PEG-M and the mixed micelles was measured by fluorimetry in the presence of pyrene, as a hydrophobic fluorescence probe, which organizes in a hydrophobic environment, changing its spectrum. The CMC values of PEG-M, PEG-M/HA_{4800} and PEG-M/HA_{14800} were 1×10^{-5} M indicating that the presence of the targeting agent did not affect the systems' ability to self-assemble. This range is similar to that calculated for other PEG-phospholipid conjugates [16,40], and is reported to be at least 100-fold lower than conventional detergents [41]. This low CMC value guarantees the retention of the micelles' physicochemical properties, and thus their integrity, even upon strong dilution.

Micelles were prepared *via* thin PEG-DSPE film hydration followed by sonication; a simple and versatile approach for self-assembling nanocarriers compared to other drug delivery systems that require a numerous procedure steps. Moreover, minimal amounts of organic solvents were used during their preparation unlike other nanosystems that were prepared through complex chemical reactions [42,43].

The derivatization of Gem with a stearoyl chain promotes hydrophobic interactions and the stable incorporation of GemC18 into the hydrophobic core of PEG-M and PEG-M/HA.

DPPE anchors to the PEG-DSPE lipid matrix during micelle formation, forming an outer HA shell without affecting the ability of the micelles to self-assemble. Unloaded micelles showed an average diameter below 50 nm, specifically ranging from 42 nm to 34 nm in the presence of HA-DPPE, and a negative zeta potential of approximately −25 mV. We found that the mean particle size of the loaded micelles was below 90 nm regardless of the presence of the HA conjugate, with PDI ranging from 0.272 to 0.315 (Table 1). The mean size was 82 nm for GemC18-PEG-M, 71 nm for GemC18-PEG-M/HA_{4800} and 68 nm for GemC18-PEG-M/HA_{14800}. Indeed, the low amount of HA-DPPE conjugate added during the preparation of actively targeted mixed micelles does not have dramatic impact on the physicochemical characteristics of the micelles. The zeta potential values were around −30 mV for all the loaded nanosystems. Moving to drug encapsulation, the presence of the HA-conjugate still guarantees high encapsulation efficiencies: 90 % and 96 % for PEG-M/HA_{4800} and PEG-M/HA_{14800}, respectively (Table 1). For all the formulations, the drug loading was about 18 %.

The ability of the micelles to retain GemC18 for an extended period of time is an important prerequisite for their use as drug delivery

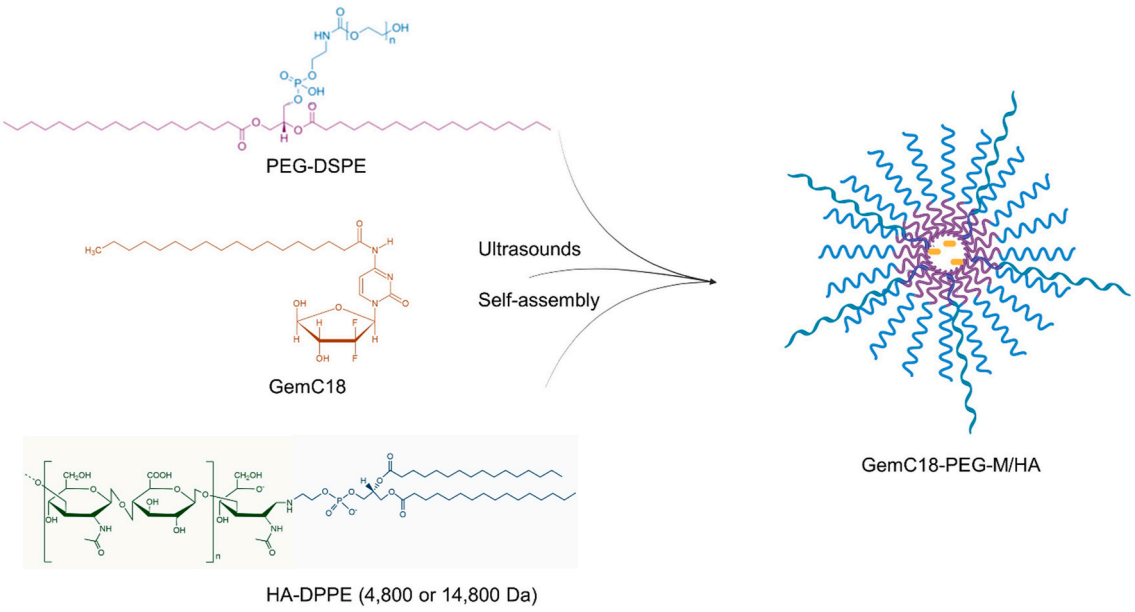

Fig. 1. Preparation process of GemC18-PEG-M/HA (created with BioRender.com).

Table 1
Physicochemical characteristics of GemC18-loaded micelles ($n = 3$).

GemC18-loaded micelles	mean diameter (nm) ± S.D.	PDI	zeta potential (mV) ± S.D.	E.E. (%)
PEG-M	82 ± 10	0.315	−29 ± 4	87 ± 10
PEG-M/HA_{4800}	71 ± 8	0.279	−31 ± 6	90 ± 4
PEG-M/HA_{14800}	68 ± 10	0.272	−27 ± 8	96 ± 3

systems. Thus, drug release was evaluated in PBS at 37 °C using a dialysis membrane. The lipophilic prodrug of Gem was retained inside the micellar matrix for an extended period of time: after an initial release of about 20 % of the loaded drug in the first hours (probably a burst effect due to the portion of GemC18 on the outer part of the micelles), PEG-M, PEG-M/HA_{4800} and PEG-M/HA_{14800} slowly released the drug and they still contained 60 % of their GemC18 after 72 h, demonstrating that GemC18 is strongly associated to the PEG-DSPE matrix.

We observed that the presence of the HA-conjugate did not affect the GemC18 release profile (Fig. S1), which was similar to that of the undecorated micelles, as has already been demonstrated for liposomal formulations [38].

The size, shape and the detailed internal structures of PEG-M/HA_{14800}, GemC18-PEG-M and GemC18-PEG-M/HA_{14800} were investigated using small angle x-ray scattering (SAXS), which is suitable for observing the arrangement of complex particles at the nanoscale [44,45]. The scattering curves I(q) for the different samples are reported in Fig. 2. In aqueous solutions, the scattering profiles of the polymer-phospholipid complexes show the typical features of nano-sized globular particles. Differences between unloaded and GemC18-loaded profiles are visible mainly in the low q region, corresponding to longer distances within the particle. A number of different models have been considered to extract detailed information about the size, shape, and internal core-shell structure of the systems.

The intensity profile of the unloaded PEG-M/HA_{14800} (1:0.4 mol) has been fitted to a core multi-shell sphere model with GENFIT software [35]. This form factor is suitable for the modelling of spherical micelles with a hydrophobic core surrounded by an extended hydrophilic shell. The fitting parameters are reported in Table 2. PEG-M/HA_{14800} shows an overall radius of 76 Å, with a hydrophobic central core of about 21 Å, compatible with the length of the C18 and C16 phospholipid saturated hydrocarbon tails. The micellar aggregation number, namely the number of PEG-HA molecules into the micellar structure, $Nagg = 4\pi R_{core}^3/3\ V_{HC}$ can be evaluated, being R_{core} the radius of the hydrophobic core and V_{HC} the volume of the hydrocarbon moiety (1016 $Å^3$ for DSPE and 960.2 $Å^3$ for DPPE). The aggregation number N_{agg} is about 40 and the interfacial area per headgroup is about 120 $Å^2$. The hydrophobic core is surrounded by a hydrophilic extended layer that can be modelled by two concentric shells, characterized by scattering length densities (Sld) higher than both the core and the solvent. The internal shell has a thickness $t_1 = 23$ Å and a Sld 9.44 10^{-6} $Å^{-2}$, while the external shell has a thickness $t_2 = 32$ Å and a Sld 9.42 10^{-6} $Å^{-2}$. The Sld decrease, observed as the distance from the core surface increases, indicates a high level of hydration of the shell, as expected for PEG and HA chains. The size of the micelle is about 154 Å, smaller than the mean hydrodynamic diameter measured by DLS, about 340 Å (PDI 1). The discrepancy may be partially due to the presence of few large aggregates in the suspension, that both could shift the average size and increase the polydispersity of the system. Moreover, the HA chains (MW 14,800 Da) have length longer than 150 Å, protruding from the micellar surface. These long hairs do not affect the SAXS profile up to long distances, due to their very low density on the surface of micelles. Rather, they may slow down the collective diffusion of micelles observed by DLS, corresponding to a calculated larger hydrodynamic size.

When GemC18 is loaded, the SAXS profile modifies compared to unloaded system, however showing an identical profile in the absence or presence of HA, as reported in Fig. 2. The scattered intensity, at constant concentration, increases compared to the unloaded micelles, suggesting the self-aggregation of the components in larger particles. Notably, in the low-q region, the intensity profiles assume a decay behaviour $I(q) \div q^{-1}$, characteristic of elongated rather than spherical particles. In the high-q region, the oscillations of the different intensity curves show similar features in all systems, indicating a core-shell internal arrangement also in the presence of GemC18. The overall structure can be modelled to a three-shell prolate ellipsoidal particle (Fig. 2C and D), with fitting parameters reported in Table 2. The hydrophobic core of the micelles shows a slight asymmetric equatorial section (a = 22 Å, b = 48 Å) and an extremely longer polar axis (c = 353 Å). The rod-like core is surrounded by a hydrophilic extended layer that can be modelled by two

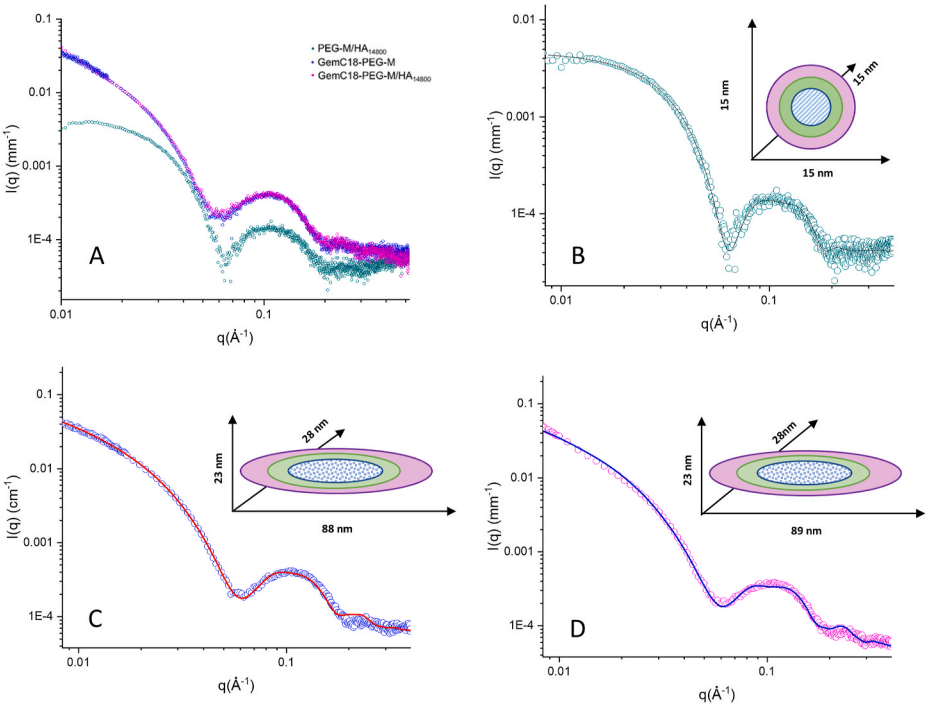

Fig. 2. SAXS intensity profiles for PEG-M/HA_{14800} (green), GemC18-PEG-M (blue) and GemC18-PEG-M/HA_{14800} (magenta). A) comparison of the different systems, B) PEG-M/HA_{14800} (green) with the best fit (solid black line) and a schematic representation of the fitting model (core-multishell sphere), C) GemC18-PEG-M (blue) with the best fit (solid red line) and a schematic representation of the fitting model (core-multishell prolate triaxial ellipsoid), GemC18-PEG-M/HA_{14800} (magenta) with the best fit (solid blue line) and a schematic representation of the fitting model (core-multishell prolate triaxial ellipsoid). Structural parameters are reported in Table 2. (For interpretation of the references to colour in this figure legend, the reader is referred to the Web version of this article.)

Table 2
Structural parameters of micelles as derived from SAXS data. Sld scattering length density, R_{core} hydrophobic core radius, a/b/c ellipsoid semiaxes, t_1 thickness of the internal hydrophilic shell, t_2 thickness of the external hydrophilic shell.

PEG-M/HA_{14800}								
Sld core (10^{-6} Å^{-2})	R core (Å)	Sld 1 (10^{-6} Å^{-2})	t_1 (Å)	Sld 2 (10^{-6} Å^{-2})	t_2 (Å)	Sld solvent (10^{-6} Å^{-2})		
9.36	22	9.44	23	9.42	32	9.41		
GemC18-PEG-M								
Sld core (10^{-6} Å^{-2})	a (Å)	b (Å)	c (Å)	Sld 1 (10^{-6} Å^{-2})	t_1 (Å)	Sld 2 (10^{-6} Å^{-2})	t_2 (Å)	Sld solvent (10^{-6} Å^{-2})
9.12	22	48	351	10.55	12	9.42	80	9.41
GemC18-PEG-M/HA_{14800}								
Sld core (10^{-6} Å^{-2})	a (Å)	b (Å)	c (Å)	Sld 1 (10^{-6} Å^{-2})	t_1 (Å)	Sld 2 (10^{-6} Å^{-2})	t_2 (Å)	Sld solvent (10^{-6} Å^{-2})
9.30	22	48	353	9.99	13	9.42	78	9.41

concentric shells, the internal one characterized by a thickness $t_1 = 13$ Å and Sld 9.99 10^{-6} Å^{-2}, and the external one by a thickness $t_2 = 75$ Å and a Sld 9.416 10^{-6} Å^{-2}. The presence of GemC18 (1:1 M ratio) changes the packing parameter of monomers within the aggregate, triggering a sphere-to-elongated transition in the overall shape of micelles. Assuming a hydrophobic volume about 500 Å^3 GemC18, it is possible to roughly estimate the aggregation number $N_{agg} = 1600$ and the mean area per molecule at the hydrophobic/hydrophilic interface A = 60 Å^2. The structural changes, both in size and shape of loaded micelles, reflect also on the hydrodynamics of the rod-like particles (axial ratio about 10), resulting in the high hydrodynamic size measured by DLS.

PXRD and FESEM were employed to investigate the crystallinity of the obtained micelles and their morphology upon dehydration. The comparison among the PXRD patterns of PEG-M/HA_{14800} (green line), GemC18-PEG-M (blue line) and GemC18-PEG-M/HA_{14800} (magenta line) is shown in Fig. 3A. The quite intense and broad signal at 2Theta=4.9° could be due to the presence of micelle. Nevertheless, the micellar organization did not affect the crystallinity of the components. Indeed, the peaks at 2Theta 15.0°, 19.1°, 21.9°, 23.2° and 26.8° are related to crystalline PEG (JCPDS file number 00-049-2095). Characteristic diffraction peaks of the PEG phase at 2Theta=19.2° and 23.2° were assigned either to the (115) and (016) [46] or (120) and (032) lattice planes [47]. The peak at 2Theta 28.4° is not typical of PEG, but it was observed in all samples: it can be reasonably due to PEG modified by the conjugation with DSPE.

It is worth noting that the peaks at 2Theta 26.7°, 31.6° and 45.3° related to the (0 0 13), (−1 1 8) and (2 0 23) crystal planes of stearic acid in the monoclinic phase (JCPDS file number 00-003-0252) were observed only in the PXRD pattern of GemC18-PEG-M (blue line) and that these signals were depleted in the presence of HA-DPPE (magenta line), which possibly indicates that the presence of HA could modify the GemC18 crystallinity.

FESEM observations pointed out the presence of elongated structures with size of about 5 μm in length and <1 μm width for both GemC18-PEG-M (Fig. 3B and Fig. S2) and GemC18-PEG-M/HA_{14800} (Fig. 3C). These structures appeared embedded in a residual matrix resulting from water evaporation. However, the morphology drastically changed in the case of PEG-M/HA_{14800}, since spherical particles with size roughly ranging between 0.5 and 1 μm were detected (Fig. 3D and detail in Fig. 3E). These features indicate that the presence of GemC18 strongly influenced the morphology of the micelles as previously observed by SAXS, in contrast to other lipid-based nanosystems [48]. It can be proposed that, during the evaporation of the sample drop, both elongated

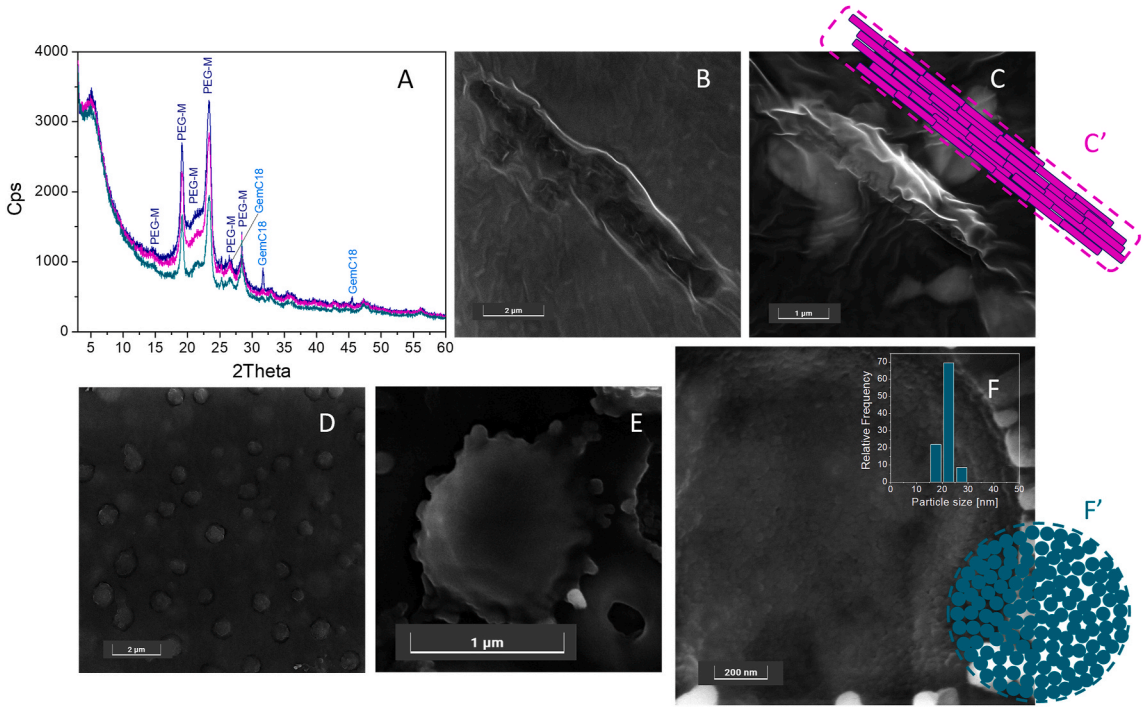

Fig. 3. A) PXRD patterns of PEG-M/HA_{14800} (green line), GemC18-PEG-M (blue line) and GemC18-PEG-M/HA_{14800} (magenta line). FESEM in-beam SE representative images of B) GemC18-PEG-M, C) GemC18-PEG-M/HA_{14800}, D), PEG-M/HA_{14800}, E) spherical superstructure of the same sample and F) spherical micelles inside the superstructure. Images collected in Ultra High-resolution mode at 5 keV, B), E) and F), and at 15 keV, C) and D). Instrumental magnification: 30000 × , 50000 × , 24000 × , 80000 × and 210000 × , respectively. Inset in F): particle size distribution of spherical micelles. Schematic representations of the elongated C') and spherical F') micelles organization. (For interpretation of the references to colour in this figure legend, the reader is referred to the Web version of this article.)

and spherical micelles self-assembled into much larger superstructures, *i.e.* supramolecular micelles which kept the single micelle original morphology, according to the occurrence of a sort of memory effect [49], as schematically depicted in Fig. 3C' and Fig. 3F'. Our hypothesis is further valorized by the observation of spherical small particles inside a spherical superstructure upon degradation under the electron beam, as shown in Fig. 3F. The average size of these small particles is d_m=21 ± 3 nm (around 210 Å), that is intermediate between the values obtained by SAXS (154 Å) and DLS (340 Å). The spherical superstructures as well as the elongated ones appeared decorated by particles of residual salts crystallized during evaporation (Fig. S3A and Fig. S4). However, looking at the EDS elemental maps shown in Fig. S3B, the spatial distributions of Na (cyan) and Cl (yellow) were not matching, conversely the map of Na overlapped the map of O (green), putting in evidence an enrichment of these elements at the surface of the spherical superstructures. Indeed, the signal related to C (red) is lower in correspondence of these particles, likely indicating the presence of this element in their internal part. This feature can be taken as an evidence that the polar heads of micelles of PEG-M/HA_{14800} are exposed in the external part and that they are able to coordinate the Na^+ ions dispersed in the solution during evaporation.

3.2. Biological validation assay

The uptake results indicate that, in Capan-1 cells, which have low levels of CD44, there were no significant differences in the uptake of fluorescently-labelled micelles, whether undecorated (NR-PEG-M) or decorated with HA_{4800}-DPPE or HA_{14800}-DPPE (NR-PEG-M/HA_{4800} or NR-PEG-M/HA_{14800}) (Fig. 4A). Similarly, in high-CD44 expressing PANC-1 cells, neither PEG-M, PEG-M/HA_{4800} or PEG-M/HA_{14800} showed any differences in uptake at the lowest dilution at any time. PEG-M/HA_{4800} and PEG-M/HA_{14800}, diluted 1:5, demonstrated time-dependent intracellular uptake which was greater with micelles diluted 1:2. Both PEG-M/HA_{4800} and PEG-M/HA_{14800} produced a significantly higher intracellular fluorescence compared to autofluorescent cells (Fig. 4B), indicating the efficient delivery of micelles cargo at these concentrations. The uptake of PEG-M/HA_{4800} or PEG-M/HA_{14800} was dependent on CD44-mediated endocytosis, as demonstrated by the reduction of the intracellular uptake of Nile Red loaded in these particles, but not in undecorated PEG-M, at the highest concentration (1:2 dilution) when CD44 highly expressing PANC-1 cells where co-incubated with a saturating amount of a CD44-neutralizing antibody or with HA, the CD44 substrate (Fig. 4C). This assay indicated that the uptake of the mixed micelles decorated with HA occurs *via* a receptor-mediated endocytosis, while the uptake of the undecorated mixed micelles occurs *via* passive diffusion.

Hence, the 1 % of HA-DPPE added during micelle formation may allow HA to expose on the surface of lipid matrix at an optimal density to bind CD44 receptor and promote GemC18 uptake to tumor site.

We next compared the cytotoxic effects of the different GemC18 prodrug-containing micelles *versus* free Gem, the first line treatment for pancreatic cancer. A time-dependent increase in cell death was observed for free Gem, GemC18, and GemC18-loaded micelles, either undecorated (GemC18-PEG-M) or decorated with HA_{4800}-DPPE or HA_{14800}-DPPE (GemC18-PEG-M/HA_{4800} or GemC18-PEG-M/HA_{14800}) at all time-points in Capan-1 cells. Free Gem had an IC_{50} > 10 µM at all time points and significantly reduced viability after 72 h. For free GemC18 the IC_{50} was below 1 µM at 48 h and 100 nM at 72 h. A significant reduction in cell viability was observed after 24 h of incubation at 10 µM, as well as after 48 h of incubation at 1 µM, for GemC18 and GemC18-loaded micelles. However, the encapsulation within micelles did not offer further advantage: indeed, the IC_{50} of GemC18-PEG-M, GemC18-PEG-M/HA_{4800} and GemC18-PEG-M/HA_{14800} was higher than that of free GemC18. At 48 h it remained >10 µM for all three formulations. At 72 h, GemC18-PEG-M and GemC18-PEG-M/HA_{4800} displayed an IC_{50} of 10 µM, while IC_{50} of GemC18-PEG-M/HA_{14800} was 100 nM (Fig. 5A). In these cells, GemC18 was the most effective drug, compared to both free Gem and GemC18-loaded micelles. It is likely that the free drug enters more promptly than micelles inducing stronger cell

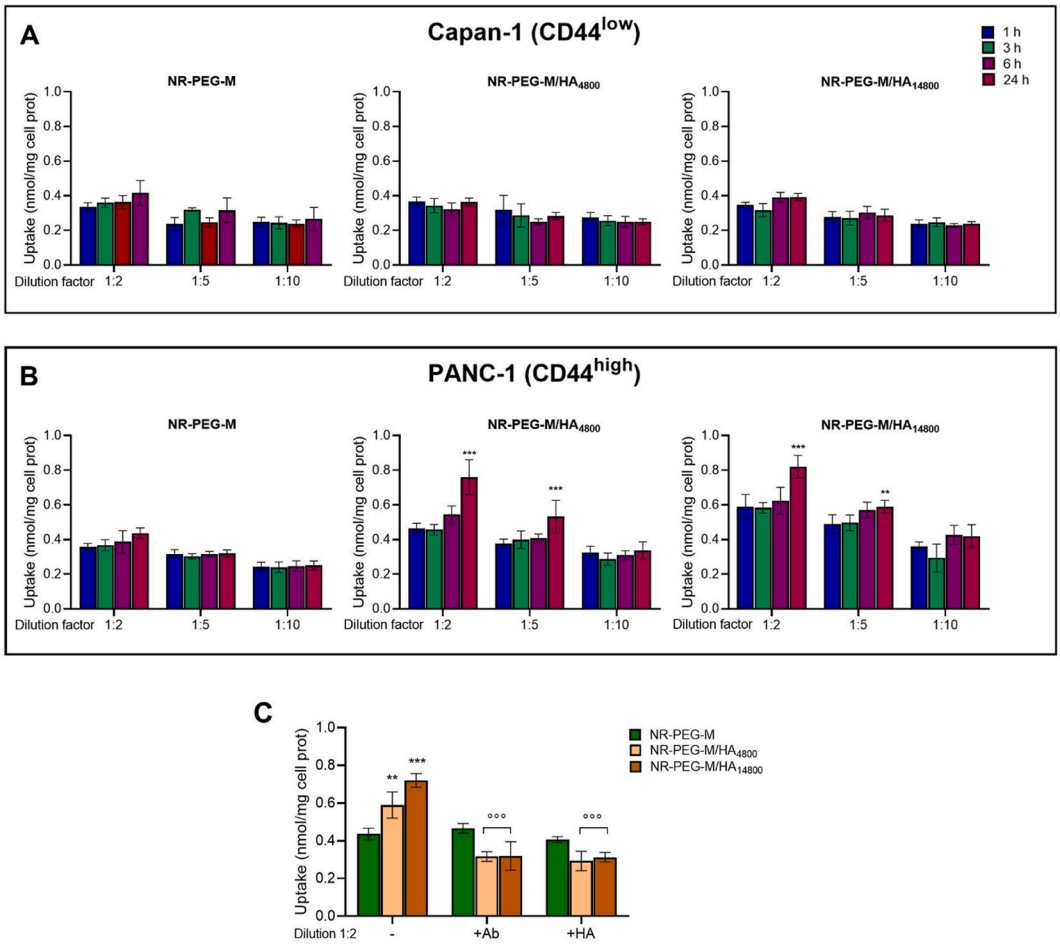

Fig. 4. (A–B) Cellular uptake by Capan-1 and PANC-1 cells of micelles, diluted 1:2, 1:5 and 1:10, labelled with Nile Red (NR), undecorated (NR-PEG-M) or decorated with PEG/HA_{4800} (NR-PEG-M/HA_{4800}) or PEG/HA_{14800} (NR-PEG-M/HA_{4800}), after 1, 3, 6 or 24 h. The autofluorescence of untreated cells was subtracted from each value. Data are presented as means ± SD (n = 3). **p < 0.01, ***p < 0.001: *vs* untreated cells. (C) PANC-1 cells were treated with micelles diluted 1:2 for 24 h, in the presence of anti-CD44 antibody diluted 1/100 (Ab) and HA (100 μM). Data are presented as means ± SD (n = 3). **p < 0.01, ***p < 0.001: *vs* untreated cells; p < 0.001: HA/Ab-treated NR-PEG-M/HA_{4800} or NR-PEG-M/HA_{14800} *vs* NR-PEG-M/HA_{4800} or NR-PEG-M/HA_{14800}. (For interpretation of the references to colour in this figure legend, the reader is referred to the Web version of this article.)

killing in this cell line. Moreover, the very low expression of CD44 implies that GemC18-PEG-M/HA_{4800} and GemC18-PEG-M/HA_{14800} offer no advantages compared to free GemC18.

In high-CD44 expressing PANC-1 cells, free Gem decreased cell viability less than in Capan-1, confirming the higher resistance of Gem of the former cells. The toxicity exerted by GemC18 and GemC18-PEG-M was like Gem; cell viability of free GemC18-treated cells at 48 and 72 h reflected increased resistance to Gem treatment: indeed, the IC_{50} of GemC18 was 10 μM and 100 nm at 48 and 72 h, respectively, while the IC_{50} of Gem was >10 μM at both time points. GemC18-PEG-M/HA_{4800} and GemC18-PEG-M/HA_{14800} were observed to be more cytotoxic relative to GemC18-PEG-M, inducing a significant reduction in cell viability in the micromolar range after 24 h, and, in the nanomolar range, after 48 and 72 h. The IC_{50} of GemC18-PEG-M was >10 μM at both 48 and 72 h; for GemC18-PEG-M/HA_{4800} it was 10 μM (48 h) and 1 μM (72 h), for GemC18-PEG-M/HA_{14800} it was 10 μM (48 h) and 100 nM (72 h), in line with the toxicity profile of GemC18 (Fig. 5B). Both GemC18-PEG-M/HA_{4800} and GemC18-PEG-M/HA_{14800} were more potent than Gem at 10 μM at all three time-points, and also at lower concentrations at 48 and 72 h. The GemC18-PEG-M/HA_{14800} formulation was more potent than GemC18-PEG-M/HA_{4800}, and was also significantly more cytotoxic than GemC18-PEG-M at the highest concentration (10 μM) at 24 h and when starting from 100 nM after 48 and 72 h. The cytotoxicity of HA-decorated micelles was dependent on their internalization *via* CD44. Indeed, when PANC-1 cells were incubated with GemC18-PEG-M/HA_{4800} and GemC18-PEG-M/HA_{14800} at the highest concentration and for the longest time with saturating amount of HA or the neutralizing anti-CD44 antibody, no cytotoxic effect was abrogated (Fig. 5C). Although both GemC18-PEG-M/HA_{4800} and GemC18-PEG-M/HA_{14800} were internalized by CD44-mediated endocytosis, the different HA-chain lengths may determine different interactions with the receptor, since the PEG-M/HA_{14800} were more internalized than the PEG-M/HA_{4800}, as suggested by the uptake assays (Fig. 4B). GemC18-PEG-M/HA_{14800} deliver the prodrug in a more efficient way than GemC18-PEG-M/HA_{4800}, resulting the more cytotoxic formulation (Fig. 5B). This behavior confirms previous observations in which liposomes decorated with HA at two different molecular weights showed different affinities for the CD44 receptor, *in vitro* and *in vivo* as a function of the increase of the polymer molecular weight [33]. The GemC18-PEG-M/HA_{14800} are also more effective than free GemC18 at 100 nM, at all the time points, while no significant differences were detected at micromolar concentrations.

Furthermore, the IC_{50} values for blank micelles exceeded 10 μM, indicating no reduction in cell viability at concentrations up to this threshold.

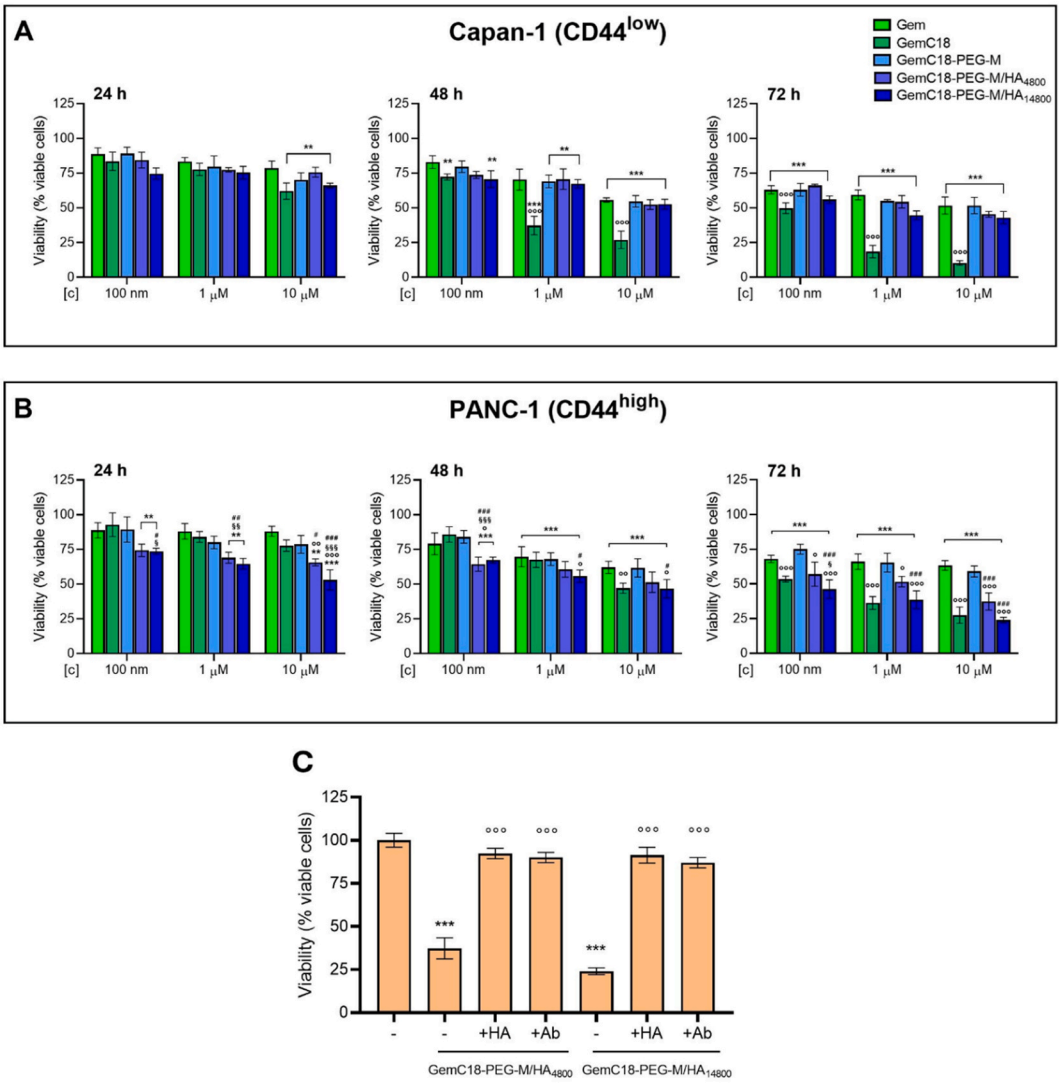

Fig. 5. (A–B) Cell viability of Capan-1 and PANC-1 cells was measured by a chemiluminescent-based commercial kit. Cells were incubated with gemcitabine (Gem), GemC18, or micelles carrying GemC18, undecorated (GemC18-PEG-M), or decorated with HA_{4800}-DPPE or HA_{14800}-DPPE (GemC18-PEG-M/HA_{4800} or GemC18-PEG-M/HA_{14800}), containing different concentrations (100 nM, 1 μM, 10 μM) of GemC18, for 24, 48 or 72 h. Cell viability of untreated cells was 100 % for all experimental conditions. Data are presented as means ± SD (n = 3). **p < 0.01, ***p < 0.001: *vs* untreated cells; °p < 0.05, °p < 0.01, p < 0.001: GemC18-PEG-M/HA_{4800} and GemC18-PEG-M/HA_{14800} *vs* Gem; §p < 0.05, §§§p < 0.001; GemC18-PEG-M/HA_{4800} or GemC18-PEG-M/HA_{14800} *vs* GemC18; #p < 0.05, ##p < 0.01, ###p < 0.001; GemC18-PEG-M/HA_{4800} or GemC18-PEG-M/HA_{14800} *vs* GemC18-PEG-M. (C) PANC-1 cells were grown for 72 h in fresh medium (−) or in the presence of GemC18-PEG-M/HA_{4800} or GemC18-PEG-M/HA_{14800} containing 10 μM GemC18, in the absence (−) or presence of HA (100 μM) or anti-CD44 antibody diluted 1/100 (Ab), then cell viability was measured. Data are presented as means ± SD (n = 3). ***p < 0.001: *vs* untreated cells; p < 0.001: HA/Ab-treated GemC18-PEG-M/HA_{4800} or GemC18-PEG-M/HA_{14800} *vs* GemC18-PEG-M/HA_{4800} or GemC18-PEG-M/HA_{14800}.

4. Conclusions

This work has demonstrated that the presence of a very low amount (1 % molar ratio) of HA-DPPE conjugate (4800 or 14,800 Da) in the PEG-DSPE micelles confers appreciable targeting ability and improves drug delivery efficiency. The Gem prodrug GemC18 was efficiently encapsulated into the micellar core, modifying the nanoparticle shape; the micelles were identified as being elongated once the amphiphilic prodrug was incorporated. *In vitro* tests on cancer cells then showed that the HA-decorated micelles display enhanced intracellular internalization and cytotoxicity towards target cells that overexpress the HA-specific receptor CD44, compared to undecorated analogs. This targeting strategy promotes enhanced binding and uptake of the HA-decorated micelles through CD44-mediated endocytosis, resulting in increased intracellular drug accumulation, specifically in resistant cells. This approach leverages both the overexpression of CD44 on cancer cells and the natural endocytic pathways to directly address drug resistance challenges. Further applications of this nanosystems could involve the co-encapsulation of multiple anticancer drugs to overcome specific resistance mechanisms. In a translational perspective, it is interesting to know that the effects of HA-decorated micelles are more pronounced in Gem-resistant cancer cells, producing a significant cytotoxic effect where Gem was ineffective. Hence, the system can set the basis of an alternative strategy to conventional Gem in pancreatic adenocarcinomas, particularly in those with high expression of CD44.

The next steps will concern the incorporation of both lipophilic and amphiphilic drugs into the PEG/HA mixed micelles to widen the number of possible applications and evaluate the influence of the drug's chemical characteristics on the shape and efficacy of the mixed micelles. This approach could then pave the way for the setup of an easily prepared platform for the targeted delivery of anticancer drugs with improved intracellular delivery.

CRediT authorship contribution statement

Ilaria Andreana: Writing – review & editing, Writing – original draft, Validation, Methodology, Investigation, Formal analysis, Data curation, Conceptualization. **Valeria Bincoletto:** Writing – review & editing, Methodology, Investigation, Data curation. **Caterina Ricci:** Writing – review & editing, Methodology, Investigation, Data curation. **Iris Chiara Salaroglio:** Writing – review & editing, Methodology, Investigation, Data curation. **Maela Manzoli:** Writing – review & editing, Supervision, Methodology, Investigation, Data curation, Conceptualization. **Beatrice Zurletti:** Writing – review & editing, Methodology, Investigation, Data curation. **Jessica Milone:** Writing – review & editing, Methodology, Investigation, Data curation. **Barbara Rolando:** Writing – review & editing, Methodology, Investigation, Data curation. **Elena Del Favero:** Writing – review & editing, Supervision, Methodology, Investigation, Data curation, Conceptualization. **Chiara Riganti:** Writing – review & editing, Supervision, Methodology, Investigation, Data curation, Conceptualization. **Pietro Matricardi:** Writing – review & editing, Supervision, Conceptualization. **Barbara Stella:** Writing – review & editing, Supervision, Project administration, Funding acquisition, Conceptualization. **Silvia Arpicco:** Writing – review & editing, Writing – original draft, Supervision, Project administration, Funding acquisition, Conceptualization.

Data availability

All data generated or analyzed during this study are included in this published article. Additional data related to this paper may be requested from the authors.

Declaration of generative AI in scientific writing

Authors did not use generative AI and AI-assisted technologies in the writing process.

Declaration of competing interest

The authors declare that they have no known competing financial interests or personal relationships that could have appeared to influence the work reported in this paper.

Acknowledgments

The authors thank ESRF for financial support and beamtime (DOI: 10.15151/ESRF-ES-1351189712), ID02 staff for technical support and PSCM facility (Grenoble) for allowing on-site sample preparation. E.D.F. thanks BIOMETRA Dept. for partial support (PSR2021_DEL_FAVERO). This work benefited from the use of the SasView application. This research was funded by Italian Ministry for University and Research (MIUR) - University of Torino, "Fondi Ricerca Locale (ex-60 %) and PRIN 2022 (grant 2022ZBZFX3).

Appendix A. Supplementary data

Supplementary data to this article can be found online at https://doi.org/10.1016/j.jddst.2024.106518.

Data availability

Data will be made available on request.

References

[1] X. Liu, Y. Cheng, Y. Mu, Z. Zhang, D. Tian, Y. Liu, X. Hu, T. Wen, Diverse drug delivery systems for the enhancement of cancer immunotherapy: an overview, Front. Immunol. 15 (2024) 1328145, https://doi.org/10.3389/fimmu.2024.1328145.

[2] E.S. Ali, S.M. Sharker, M.T. Islam, I.N. Khan, S. Shaw, M.A. Rahman, S.J. Uddin, M. C. Shill, S. Rehman, N. Das, et al., Targeting cancer cells with nanotherapeutics and nanodiagnostics: current status and future perspectives, Semin. Cancer Biol. 69 (2021) 52–68, https://doi.org/10.1016/j.semcancer.2020.01.011.

[3] G. Wei, Y. Wang, G. Yang, Y. Wang, R. Ju, Recent progress in nanomedicine for enhanced cancer chemotherapy, Theranostics 11 (2021) 6370–6392, https://doi.org/10.7150/thno.57828.

[4] F. Rommasi, N. Esfandiari, Liposomal nanomedicine: applications for drug delivery in cancer therapy, Nanoscale Res. Lett. 16 (2021) 95, https://doi.org/10.1186/s11671-021-03553-8.

[5] Z. Edis, J. Wang, M.K. Waqas, M. Ijaz, M. Ijaz, Nanocarriers-mediated drug delivery systems for anticancer agents: an overview and perspectives, Int J Nanomedicine 16 (2021) 1313–1330, https://doi.org/10.2147/ijn.S289443.

[6] D. Hwang, J.D. Ramsey, A.V. Kabanov, Polymeric micelles for the delivery of poorly soluble drugs: from nanoformulation to clinical approval, Adv. Drug Deliv. Rev. 156 (2020) 80–118, https://doi.org/10.1016/j.addr.2020.09.009.

[7] Y. Yuan, W. Tan, Y. Mi, L. Wang, Z. Qi, Z. Guo, Effect of hydrophobic chain length in amphiphilic chitosan conjugates on intracellular drug delivery and smart drug release of redox-responsive micelle, Mar. Drugs 22 (2023), https://doi.org/10.3390/md22010018.

[8] A. Phungula, A.Y. Waddad, M.D. Fernandez Leyes, P. Di Gianvincenzo, B. Espuche, S. Zuffi, S.E. Moya, F. Albericio, B.G. de la Torre, Self-assembly of NrTP6 cell-penetrating lipo-peptide with variable number of lipid chains: impact of phosphate ions on lipid association, J. Colloid Interface Sci. 654 (2024) 124–133, https://doi.org/10.1016/j.jcis.2023.09.161.

[9] C. Wang, H. Zhao, Polymer brushes and surface nanostructures: molecular design, precise synthesis, and self-assembly, Langmuir (2024), https://doi.org/10.1021/acs.langmuir.3c02813.

[10] X. Wang, Y. Wang, T. Tang, G. Zhao, W. Dong, Q. Li, X. Liang, Curcumin-loaded RH60/F127 mixed micelles: characterization, biopharmaceutical characters and anti-inflammatory modulation of airway inflammation, Pharmaceutics 15 (2023), https://doi.org/10.3390/pharmaceutics15122710.

[11] M. Zhang, N. Ying, J. Chen, L. Wu, H. Liu, S. Luo, D. Zeng, Engineering a pH-responsive polymeric micelle co-loaded with paclitaxel and triptolide for breast cancer therapy, Cell Prolif. (2024) e13603, https://doi.org/10.1111/cpr.13603.

[12] J. Liu, Y. Zhang, C. Liu, Y. Jiang, Z. Wang, X. Li, Paclitaxel prodrug-encapsulated polypeptide micelles with redox/pH dual responsiveness for cancer chemotherapy, Int J Pharm 645 (2023) 123398, https://doi.org/10.1016/j.ijpharm.2023.123398.

[13] C. Xu, Y. Ding, J. Ni, L. Yin, J. Zhou, J. Yao, Tumor-targeted docetaxel-loaded hyaluronic acid-quercetin polymeric micelles with p-gp inhibitory property for hepatic cancer therapy, RSC advances 6 (2016) 27542–27556, https://doi.org/10.1039/C6RA00460A.

[14] M. Huo, H. Wang, Y. Zhang, H. Cai, P. Zhang, L. Li, J. Zhou, T. Yin, Co-delivery of silybin and paclitaxel by dextran-based nanoparticles for effective anti-tumor treatment through chemotherapy sensitization and microenvironment modulation, J Control Release 321 (2020) 198–210, https://doi.org/10.1016/j.jconrel.2020.02.017.

[15] Q. Yang, K.R. Moulder, M.S. Cohen, S. Cai, L.M. Forrest, Cabozantinib loaded DSPE-PEG(2000) micelles as delivery system: formulation, characterization and cytotoxicity evaluation, BAOJ Pharm Sci 1 (2015).

[16] A.N. Lukyanov, V.P. Torchilin, Micelles from lipid derivatives of water-soluble polymers as delivery systems for poorly soluble drugs, Adv. Drug Deliv. Rev. 56 (2004) 1273–1289, https://doi.org/10.1016/j.addr.2003.12.004.

[17] B. Xu, Z. Ding, Y. Hu, T. Zhang, S. Shi, G. Yu, X. Qi, Preparation and evaluation of the cytoprotective activity of micelles with DSPE-PEG-C60 as a carrier against doxorubicin-induced cytotoxicity, Front. Pharmacol. 13 (2022) 952800, https://doi.org/10.3389/fphar.2022.952800.

[18] P. Graván, J. Peña-Martín, J.L. de Andrés, M. Pedrosa, M. Villegas-Montoya, F. Galisteo-González, J.A. Marchal, P. Sánchez-Moreno, Exploring the impact of nanoparticle stealth coatings in cancer models: from PEGylation to cell membrane-coating nanotechnology, ACS Appl. Mater. Interfaces 16 (2024) 2058–2074, https://doi.org/10.1021/acsami.3c13948.

[19] E. Blanco, H. Shen, M. Ferrari, Principles of nanoparticle design for overcoming biological barriers to drug delivery, Nat. Biotechnol. 33 (2015) 941–951, https://doi.org/10.1038/nbt.3330.

[20] Y. Takakura, Y. Takahashi, Strategies for persistent retention of macromolecules and nanoparticles in the blood circulation, J Control Release 350 (2022) 486–493, https://doi.org/10.1016/j.jconrel.2022.05.063.

[21] Q. Guo, L. Zhang, M. He, X. Jiang, J. Tian, Q. Li, Z. Liu, L. Wang, H. Sun, Doxorubicin-loaded natural daptomycin micelles with enhanced targeting and anti-tumor effect in vivo, Eur. J. Med. Chem. 222 (2021) 113582, https://doi.org/10.1016/j.ejmech.2021.113582.

[22] Q. Du, F. Lv, J. Huang, X. Tang, Z. Zhao, J. Chen, A multiple environment-sensitive prodrug nanomicelle strategy based on chitosan graftomer for enhanced tumor therapy of gambogic acid, Carbohydr. Polym. 267 (2021) 118229, https://doi.org/10.1016/j.carbpol.2021.118229.

[23] Y. Zheng, Y. Oz, Y. Gu, N. Ahamad, K. Shariati, J. Chevalier, D. Kapur, N. Annabi, Rational design of polymeric micelles for targeted therapeutic delivery, Nano Today 55 (2024), https://doi.org/10.1016/j.nantod.2024.102147.

[24] R.K. Sironen, M. Tammi, R. Tammi, P.K. Auvinen, M. Anttila, V.M. Kosma, Hyaluronan in human malignancies, Exp. Cell Res. 317 (2011) 383–391, https://doi.org/10.1016/j.yexcr.2010.11.017.

[25] H.-J. Cho, Recent progresses in the development of hyaluronic acid-based nanosystems for tumor-targeted drug delivery and cancer imaging, Journal of pharmaceutical investigation 50 (2020) 115–129, https://doi.org/10.1007/s40005-019-00448-w.

[26] H.A. Burris 3rd, M.J. Moore, J. Andersen, M.R. Green, M.L. Rothenberg, M. R. Modiano, M.C. Cripps, R.K. Portenoy, A.M. Storniolo, P. Tarassoff, et al., Improvements in survival and clinical benefit with gemcitabine as first-line therapy for patients with advanced pancreas cancer: a randomized trial, J. Clin. Oncol. 41 (2023) 5482–5492, https://doi.org/10.1200/jco.22.02777.

[27] M.L. Immordino, P. Brusa, F. Rocco, S. Arpicco, M. Ceruti, L. Cattel, Preparation, characterization, cytotoxicity and pharmacokinetics of liposomes containing lipophilic gemcitabine prodrugs, J Control Release 100 (2004) 331–346, https://doi.org/10.1016/j.jconrel.2004.09.001.

[28] L. Neutsch, E.M. Wirth, S. Spijker, C. Pichl, H. Kählig, F. Gabor, M. Wirth, Synergistic targeting/prodrug strategies for intravesical drug delivery–lectin-modified PLGA microparticles enhance cytotoxicity of stearoyl gemcitabine by contact-dependent transfer, J Control Release 169 (2013) 62–72, https://doi.org/10.1016/j.jconrel.2013.04.004.

[29] M. Bartkowski, V. Bincoletto, I.C. Salaroglio, G. Ceccone, R. Arenal, S. Nervo, B. Rolando, C. Riganti, S. Arpicco, S. Giordani, Enhancing pancreatic ductal adenocarcinoma (PDAC) therapy with targeted carbon nano-onion (CNO)-mediated delivery of gemcitabine (GEM)-derived prodrugs, J. Colloid Interface Sci. 659 (2024) 339–354, https://doi.org/10.1016/j.jcis.2023.12.166.

[30] S. Zhu, P. Wonganan, D.S. Lansakara-P, H.L. O'Mary, Y. Li, Z. Cui, The effect of the acid-sensitivity of 4-(N)-stearoyl gemcitabine-loaded micelles on drug resistance caused by RRM1 overexpression, Biomaterials 34 (2013) 2327–2339, https://doi.org/10.1016/j.biomaterials.2012.11.053.

[31] Z. Daman, S. Ostad, M. Amini, K. Gilani, Preparation, optimization and in vitro characterization of stearoyl-gemcitabine polymeric micelles: a comparison with its self-assembled nanoparticles, Int J Pharm 468 (2014) 142–151, https://doi.org/10.1016/j.ijpharm.2014.04.021.

[32] Y. Wang, W. Fan, X. Dai, U. Katragadda, D. McKinley, Q. Teng, C. Tan, Enhanced tumor delivery of gemcitabine via PEG-DSPE/TPGS mixed micelles, Mol. Pharm. 11 (2014) 1140–1150, https://doi.org/10.1021/mp4005904.

[33] S. Arpicco, C. Lerda, E. Dalla Pozza, C. Costanzo, N. Tsapis, B. Stella, M. Donadelli, I. Dando, E. Fattal, L. Cattel, et al., Hyaluronic acid-coated liposomes for active targeting of gemcitabine, Eur. J. Pharm. Biopharm. 85 (2013) 373–380, https://doi.org/10.1016/j.ejpb.2013.06.003.

[34] Z. Song, R. Feng, M. Sun, C. Guo, Y. Gao, L. Li, G. Zhai, Curcumin-loaded PLGA-PEG-PLGA triblock copolymeric micelles: preparation, pharmacokinetics and distribution in vivo, J. Colloid Interface Sci. 354 (2011) 116–123, https://doi.org/10.1016/j.jcis.2010.10.024.

[35] F. Spinozzi, C. Ferrero, M.G. Ortore, A. De Maria Antolinos, P. Mariani, GENFIT: software for the analysis of small-angle X-ray and neutron scattering data of macromolecules in solution, J. Appl. Crystallogr. 47 (2014) 1132–1139, https://doi.org/10.1107/s1600576714005147.

[36] M.E. Cano, D. Lesur, V. Bincoletto, E. Gazzano, B. Stella, C. Riganti, S. Arpicco, J. Kovensky, Synthesis of defined oligohyaluronates-decorated liposomes and interaction with lung cancer cells, Carbohydr. Polym. 248 (2020) 116798, https://doi.org/10.1016/j.carbpol.2020.116798.

[37] H. Xu, M. Niu, X. Yuan, K. Wu, A. Liu, CD44 as a tumor biomarker and therapeutic target, Exp. Hematol. Oncol. 9 (2020) 36, https://doi.org/10.1186/s40164-020-00192-0.

[38] E. Gazzano, I. Buondonno, A. Marengo, B. Rolando, K. Chegaev, J. Kopecka, S. Saponara, M. Sorge, C.M. Hattinger, A. Gasco, et al., Hyaluronated liposomes containing H2S-releasing doxorubicin are effective against P-glycoprotein-positive/doxorubicin-resistant osteosarcoma cells and xenografts, Cancer Lett. 456 (2019) 29–39, https://doi.org/10.1016/j.canlet.2019.04.029.

[39] I. Andreana, V. Bincoletto, M. Manzoli, F. Rodà, V. Giarraputo, P. Milla, S. Arpicco, B. Stella, Freeze drying of polymer nanoparticles and liposomes exploiting different saccharide-based approaches, Materials 16 (2023), https://doi.org/10.3390/ma16031212.

[40] Z. Sezgin, N. Yüksel, T. Baykara, Preparation and characterization of polymeric micelles for solubilization of poorly soluble anticancer drugs, Eur. J. Pharm. Biopharm. 64 (2006) 261–268, https://doi.org/10.1016/j.ejpb.2006.06.003.

[41] M.J. Rosen, J.T. Kunjappu, Surfactants and Interfacial Phenomena, John Wiley & Sons, 2012.

[42] X. He, Z. Jiang, O.U. Akakuru, J. Li, A. Wu, Nanoscale covalent organic frameworks: from controlled synthesis to cancer therapy, Chem. Commun. 57 (2021) 12417–12435, https://doi.org/10.1039/d1cc04846e.

[43] C. Zhao, X. Tang, X. Chen, Z. Jiang, Multifaceted carbonized metal-organic frameworks synergize with immune checkpoint inhibitors for precision and augmented cuproptosis cancer therapy, ACS Nano 18 (2024) 17852–17868, https://doi.org/10.1021/acsnano.4c04022.

[44] E. Di Cola, L. Cantu, P. Brocca, V. Rondelli, G.C. Fadda, E. Canelli, P. Martelli, A. Clementino, F. Sonvico, R. Bettini, et al., Novel O/W nanoemulsions for nasal administration: structural hints in the selection of performing vehicles with enhanced mucopenetration, Colloids Surf. B Biointerfaces 183 (2019) 110439, https://doi.org/10.1016/j.colsurfb.2019.110439.

[45] C.I. Camara, L. Bertocchi, C. Ricci, R. Bassi, A. Bianchera, L. Cantu, R. Bettini, E. Del Favero, Hyaluronic acid-dexamethasone nanoparticles for local adjunct therapy of lung inflammation, Int. J. Mol. Sci. 22 (2021), https://doi.org/10.3390/ijms221910480.

[46] Y. Li, X. Li, F. Xiang, T. Huang, Y. Wang, J. Wu, Z. Zhou, Crystallization, rheological, and mechanical properties of PLLA/PEG blend with multiwalled carbon nanotubes, Polym. Adv. Technol. 22 (2011) 1959–1970, https://doi.org/10.1002/pat.1702.

[47] R. Li, Y. Wu, Z. Bai, J. Guo, X. Chen, Effect of molecular weight of polyethylene glycol on crystallization behaviors, thermal properties and tensile performance of polylactic acid stereocomplexes, RSC Adv. 10 (2020) 42120–42127, https://doi.org/10.1039/d0ra08699a.

[48] R. Bahramabadi, H. Hakimi, A. Saljooqi, M. Barani, D. Razmjoue, M. Zare-Bidaki, M. Mohamadi, The essential oil of rocket seeds maintains its antibacterial effects after encapsulation in nanoliposomes, J. Herb. Med. 47 (2024) 100924, https://doi.org/10.1016/j.hermed.2024.100924.

[49] D. Wang, G. Tong, R. Dong, Y. Zhou, J. Shen, X. Zhu, Self-assembly of supramolecularly engineered polymers and their biomedical applications, Chem. Commun. 50 (2014) 11994–12017, https://doi.org/10.1039/c4cc03155e.